Extensive flow cytometric immunophenotyping of human PBMC incorporating detection of chemokine receptors, cytokines and tetramers

Wolfswinkel, M. van; Meijgaarden, K.E. van; Ottenhoff, T.H.M.; Niewold, P.; Joosten, S.A.

Received: 1 September 2022 | Revised: 19 January 2023 | Accepted: 24 February 2023

DOI: 10.1002/cyto.a.24727

TECHNICAL NOTE

MIFlowCyt

ISAC INTERNATIONAL SOCIETY FOR ADVANCEMENT OF CYTOMETRY

CYTOMETRY Journal of Quantitative Cell Science PART A

Extensive flow cytometric immunophenotyping of human PBMC incorporating detection of chemokine receptors, cytokines and tetramers

Marjolein van Wolfswinkel | Krista E. van Meijgaarden | Tom H. M. Ottenhoff | Paula Niewold | Simone A. Joosten

Department of Infectious Diseases, Leiden University Medical Center, The Netherlands

Correspondence
Paula Niewold, Department of Infectious Diseases, Leiden University Medical Center, PO Box 9600, 2300 RC Leiden, The Netherlands.
Email: p.niewold@lumc.nl

Funding information
National Institutes of Health

Abstract

Characterization of immune cells is essential to advance our understanding of immunology and flow cytometry is an important tool in this context. Addressing both cellular phenotype and antigen-specific functional responses of the same cells is valuable to achieve a more integrated understanding of immune cell behavior and maximizes information obtained from precious samples. Until recently, panel size was limiting, resulting in panels generally focused on either deep immunophenotyping or functional readouts. Ongoing developments in the field of (spectral) flow cytometry have made panels of 30^{+} markers more accessible, opening up possibilities for advanced integrated analyses. Here, we optimized immune phenotyping by co-detection of markers covering chemokine receptors, cytokines and specific T cell/peptide tetramer interaction using a 32-color panel. Such panels enable integrated analysis of cellular phenotypes and markers assessing the quality of immune responses and will contribute to our understanding of the immune system.

KEYWORDS
antigen-specific responses, broad immunophenotyping, chemokine receptors, cytokine detection, high-dimensional flow cytometry, intracellular staining, spectral flow cytometry, tetramer staining

1 | INTRODUCTION

The human immune system is complex and to understand the pathogenesis of infectious diseases, autoimmunity and cancer it is essential to characterize the cells involved. Immune phenotyping by flow cytometry is one of the available tools and has contributed many insights since its inception in 1968 [1]. As our knowledge of immune markers and cellular phenotypes is increasing, so is the number of markers required for accurate cell phenotyping. Recent developments of (spectral) flow cytometry technology and associated fluorophore availability have made high-dimensional flow cytometry more accessible [2]. New challenges associated with designing 30+ parameter flow cytometry panels are being tackled by many immunologists and companies resulting in the development of larger 'optimized multicolour immunofluorescence panels' (OMIP) [3–5]. OMIP-069 elegantly

Marjolein van Wolfswinkel, Krista E. van Meijgaarden, Paula Niewold and Simone A. Joosten contributed equally to this work.

The content is solely the responsibility of the authors and does not necessarily represent the official views of the National Institutes of Health. The funders had no role in study design, data collection and analysis, decision to publish, or preparation of the manuscript.

described the use of 40 colors for deep immunophenotyping of human peripheral blood, and with this and similar panels one can detect all known major cell subsets [5–8]. However, to comprehensively study antigen-specific responses, which is pivotal to understanding disease outcomes, measurement of cytokines or addition of tetramers to immunophenotyping panels is required [9–12]. Unfortunately, additional markers often cannot simply be added to existing panels as this may impact panel performance. Therefore, we aimed to develop and optimize a panel combining detailed immunophenotyping with assessment of antigen-specific responses.

In this panel, a tetramer, two cytokines and several surface markers have been added to general phenotyping markers to assess antigen-specific responses within the context of broader immune characterization. Tetramers are great tools to enumerate antigen specific T-cells and are available for many MHC class I alleles. Although this paper focusses on HLA-E specific tetramers, as that is our particular research interest, the workflow developed here should be applicable to other tetramers as well. HLA-E presented peptides are of particular interest for vaccine development as the HLA-E molecule is a non-polymorphic class 1b molecule and therefore considered an interesting antigen presentation molecule to target responses in the global population [13, 14]. HLA-E plays a role in the innate immune system, by presenting signal sequence peptides from class Ia alleles to the NKG2A/CD94 complex to inhibit NK mediated lysis, but also serves as antigen presentation molecule for pathogen derived peptides to T cells in the adaptive immune response [15]. Prezzemolo et al. described the ex vivo detection of HLA-E-peptide specific T cells by HLA-E tetramers in combination with cytokines, using smaller, partially overlapping, panels of up to 12 markers [12].

The markers incorporated in the panel reported here were selected to identify the main leukocyte lineages in the blood (B cells, T cells, NK cells, monocytes) as well as their differentiation and activation status. The following lineage markers were included: CD19 and CD20 for the identification of B cells, CD14 for monocytes, CD56 for NK cells and CD3, CD4, CD8, TCRαβ and TCRγδ for the main T cell populations [16]. Co-expression of CD3 and CD56 can be used to identify NKT cells [17]. Next, markers required to refine differentiation status or identify additional subsets within these lineages were incorporated. Within the NK cell population differentiation is defined by CD16 and CD56 expression, while for B cells CD27 and IgD are used to identify naive and class-switched subsets [18–20]. Monocytes are subdivided into classical, non-classical and intermediate subsets based on CD14 and CD16 in combination with CCR2 and CX3CR1 expression [21–23]. CD45RA and CCR7 were included to aid classification of T cells into naive, central memory, effector memory and terminal effector memory populations, and CD27 and CD28 to identify the differentiation stages within these populations [24, 25]. In addition CXCR3, CCR4 and CCR6 were incorporated to distinguish Th1, Th2 and Th17 T cells, respectively [24, 26]. CD95 was included as a marker for antigen-activated T or stem cell-like memory T cells, and CD62L was added as a homing marker [27]. CD25 identifies regulatory T cells as well as activated B and T cells, and HLA-DR is expressed on monocytes, B cells and activated T cells [16, 24]. CD38 expression is found on monocytes, NK-, T- and B cells [16]. NKG2A is an inhibitory receptor expressed on NK cells, while NKG2C is an activation receptor within this lineage [18]. CD85d and CD85j are inhibitory receptors for HLA-molecules which can be expressed by both monocytes and B cells [28–31]. To address antigen-specific responses HLA-E/*Mycobacterium tuberculosis*-peptide tetramer was incorporated, while antigen-induced cytokine production was assessed by intracellular detection of IFN-γ and TNF-α.

Here, we describe a 32-color panel consisting of 23 markers phenotyping most major cell subsets in human PBMC samples, and 9 additional markers addressing HLA-E specific T cell interactions and cytokine production. This paper addresses the optimization of a panel combining chemokine receptors, surface markers, cytokines and tetramers. Development of this workflow enables immunophenotyping of human PBMC while measuring cytokine production of antigen-specific cells, thus allowing for comprehensive assessment of cellular phenotype and function within the same sample.

2 | MATERIALS AND METHODS

2.1 | Donors

Samples used in these experiments were obtained from buffy coats collected from anonymous healthy blood bank donors (Sanquin Bloodbank, the Netherlands), with informed consent. Peripheral blood mononuclear cells (PBMC) were isolated by Ficoll-Amidotrizoate (Pharmacy LUMC, Leiden, The Netherlands) density centrifugation, cryopreserved in Roswell Park Memorial Institute (RPMI) 1640 medium (Thermo Fischer, Life Technologies Europe B.V., Bleiswijk, The Netherlands) containing 20% fetal bovine serum (FBS; Capricorn Scientific, Ebsdorfergrund, Germany) and 10% dimethyl sulfoxide (DMSO; Honeywell, Seelze, Germany) and stored in liquid nitrogen until further analysis. Experiments for panel optimization were performed on three to five donors and the panel was validated on PBMC from an additional 5 independent donors.

2.2 | Sample preparation and stimulation

PBMC samples were thawed and rested for 90 min in RPMI/10% FBS with 0.2 mg/mL DNase I (Roche Diagnostics GmbH, Mannheim, Germany) at 37°C with 5% CO_2. Cells were washed (10 min, 450 x g) and counted with the CASY cell counter (Roche Diagnostics GmbH, Mannheim, Germany).

Cells were stimulated at 4 x 10^6 cells/mL with 2 μg/mL of staphylococcal enterotoxin B (SEB; Toxin Technology, Sarasota, USA) in RPMI/10% FBS in 5 mL round-bottom tubes. Brefeldin A (3 μg/mL, Merck KGaA, Darmstadt, Germany) and monensin (1:1000, BioLegend, Amsterdam, The Netherlands) were added after 6 h and cells were left overnight at 37°C with 5% CO_2. Cells were then harvested and washed with phosphate buffered saline (PBS; Fresenius Kabi Nederland B.V., Huis ter Heide, The Netherlands).

For stimulation with phorbol myristate acetate (PMA; Focus Biomolecules, Plymouth Meeting, USA) and Ionomycin (Focus Biomolecules, Plymouth Meeting, USA), cells were stimulated at 4 x 10^6 cells/mL with 400 ng/mL of Ionomycin and 5 ng/mL of PMA in RPMI/10% FBS in 5 mL round-bottom tubes. Brefeldin A (3 μg/mL) and monensin (1:1000) were added after 2 h and cells were left at 37°C with 5% CO_2 for 4 h in total. Cells were then harvested and washed with phosphate buffered saline (PBS; Fresenius Kabi Nederland B.V., Huis ter Heide, The Netherlands).

2.3 | Flow cytometry basic optimization and marker description

Antibody titration, reference control optimization, autofluorescence correction and the addition of the Brilliant Stain buffer and True-Stain Monocyte Blocker were performed as described in OMIP-069 [5]. Cells rather than beads were used as reference controls to minimize unmixing inaccuracies [5]. For less abundant markers, such as TCRγδ and tetramer, at least 5 x 10^5 events were acquired to accurately determine the positive population. All antibodies were titrated separately but the final concentration used was adapted, if needed, based on comparison of the single stain to a fully stained sample. Monocyte autofluorescence was corrected using the autofluorescence extraction option on the Aurora flow cytometer. Fluorescence minus one (FMO) controls were used to evaluate and solve final unmixing errors and spread impact. Detailed information on markers, clones, dilutions and manufacturers is provided in Table SS1. Due to availability issues with Pacific Orange CD20 (HI47), this antibody was replaced with the BV570 CD20 (2H7) antibody. Therefore the donor shown in Figure 1 and Figure SS1 and SS2 is stained with the Pacific Orange CD20 and the donors shown in Figure 3, 4 and Figure SS3 and SS4 were stained with BV570 CD20. HLA-E*01:03 tetramers were produced in-house as previously described [12, 32], and loaded with Mtb-peptides 34 (VMTTVLATL) or 62 (RMPPLGHEL) [33].

2.4 | Flow cytometry staining

Approximately 2 x 10^6 cells per sample were stained with a live/dead marker according to manufacturer's instructions (Invitrogen Live/Dead Fixable Blue, Thermo Fischer, Life Technologies Europe B.V., Bleiswijk, The Netherlands) and blocked with 10 μg/mL purified CD94 mAb (Clone HP-3D9, BD Biosciences, Erembodegem, Belgium) in PBS for 30 min at room temperature (RT) in the dark. Cells were then washed (5 min, 450 x g) with PBS containing 0.1% bovine serum albumin (BSA; Roche Diagnostics GmbH, Mannheim, Germany), blocked with 5% pooled normal human serum in PBS for 10 min at RT to block Fc receptors and washed once with PBS/0.1% BSA. Cells were subsequently incubated with a cocktail containing True-Stain Monocyte Blocker™ (1:20, BioLegend, Amsterdam, The Netherlands), Brilliant Stain Buffer Plus (1:10, BD Biosciences, Erembodegem, Belgium) and chemokine receptor antibodies (CCR2, CCR4, CCR6, CCR7, CXCR3 and CX3CR1) in PBS/0.1% BSA for 30 min at 37°C in the dark. After incubation, cells were washed once with PBS/0.1% BSA. When tetramer staining was performed, cells were incubated with a combination of two HLA-E tetramers (5.4 μg/mL per tetramer) in PBS/0.1% BSA for 30 min at 37°C in the dark, washed once with PBS/0.1% BSA, fixed with 1% paraformaldehyde (Pharmacy LUMC, Leiden, The Netherlands) for 10 min at RT and washed once with PBS/0.1% BSA. Cells were subsequently stained with a cocktail containing Brilliant Stain Buffer Plus (1:10) and the surface antibodies CD3, CD4, CD8, CD14, CD16, CD19, CD20, CD25, CD27, CD28, CD38, CD45RA, CD56, CD62L, CD85d, CD85j, CD95, HLA-DR, IgD, NKG2a, NKG2c, TCRαβ and TCRγδ in PBS/0.1% BSA for 30 min at 4°C in the dark. Upon PMA/ionomycin stimulation, CD3, CD4 and CD8 were not included in the surface staining cocktail, but in the ICS staining. After incubation, cells were washed twice with PBS/0.1% BSA. When ICS was performed, cells were fixed for 15 min at RT with fixation medium A (Nordic MUbio, Susteren, The Netherlands), washed twice with PBS/0.1% BSA and stained with ICS antibodies IFN-γ and TNF-α in permanent non-saponin based permeabilization medium B (Nordic MUbio, Susteren, The Netherlands) for 30 min at RT in the dark. Cells were washed twice with PBS/0.1% BSA at 650 x g followed by fixation with 1% paraformaldehyde for 10 min at RT. Cells were washed twice with PBS/0.1% BSA, resuspended in PBS/0.1% BSA and acquired on a 5 L Cytek®Aurora (Cytek Biosciences, Fremont, CA, USA) at the Flow cytometry Core Facility (FCF) of Leiden University Medical Center (LUMC) in Leiden, Netherlands.

2.5 | Data analysis

Data was analyzed using FlowJo v10.8.0 and OMIQ analysis software (www.omiq.ai). Within OMIQ, the data was first manually gated to remove debris, aggregates and dead cells. On the live singlets, a UMAP followed by a FlowSOM was performed to visualize and cluster the data. All markers except the live/dead stain, tetramer, IFN-γ and TNF-α were included in the UMAP settings. A heatmap was generated to translate the clusters to known cell populations. Only clusters with >100 cells were included for visualization.

3 | RESULTS

The possibilities for multiparameter flow cytometry are rapidly expanding and developing, and optimizing a panel tailored to specific research questions presents challenges. Here, the workflow to optimize simultaneous detection of cell lineage markers, activation markers, chemokine receptors, peptide–MHC tetramers and intracellular cytokines is described. As each of these markers and analytes has their own characteristics and requirements, staining for each marker category was optimized separately, prior to incorporation into the combined protocol. The panel (Table 1) was optimized on PBMC samples from healthy blood bank donors, which were stimulated with staphylococcal enterotoxin B (SEB) to analyze performance of surface

markers as well as cytokine production in combination with HLA-E peptide specific tetramer frequencies.

3.1 | Chemokine receptors

Firstly, the impact of temperature on staining intensity and separation of positive and negative populations of chemokine receptors CCR2, CCR4, CCR6, CCR7, CXCR3 and CX3CR1 was tested at 4°C vs 37°C (Figure 1A). For CCR2, CCR4, CCR7 and CXCR3 staining at 37°C increased sensitivity and separation of the positive signal (MFI $CCR2^+$ 6413 (4°C) vs 12,658 (37°C); MFI $CCR4^+$ 6731 (4°C) vs 10,033 (37°C); MFI $CCR6^+$ 2192 (4°C) vs 2620 (37°C); MFI $CCR7^+$ 2347 (4°C) vs 4352 (37°C); MFI $CXCR3^+$ 1122 (4°C) vs 1485 (37°C)). For CX3CR1, the advantages in staining intensity when staining at 37°C were limited but does not favor staining at 4°C either (MFI $CX3CR1^+$ 1525 (4°C) vs 1766 (37°C)). For all chemokine receptors, except CX3CR1, the negative population did not differ from the unstained sample when staining was performed at either 4 or 37°C. For CX3CR1 a minimal shift of the negative population was observed irrespective of the staining temperature.

3.2 | Tetramer staining

Optimal detection of peptide-specific T cell frequencies with tetramers on PBMC samples is performed at 37°C [12]. To specifically investigate HLA-E - T cell interactions, HLA-E tetramer staining protocols include blocking of CD94 molecule to prevent tetramer HLA-E - NKG2/CD94 interactions [12]. To prevent loss of tetramer signal, a fixation step is performed immediately after tetramer staining, before staining of the remaining surface markers [34]. This fixation step did not notably impact the resolution of markers added in the subsequent staining steps (Figure S1). The effect of simultaneous staining on the performance of tetramers and chemokine receptors (CCRs) on T cells is shown in Figure 1B,C. PBMC samples were stained with the full surface panel including either only tetramer staining, only CCR staining (with CCR2, CCR4, CCR6, CCR7, CXCR3 and CX3CR1) or combined in the following order; simultaneous staining of tetramer and CCRs, staining tetramer first and CCRs second and vice versa. As performance of the tetramer and CCR4 were impacted most by the staining order, representative dot plots of these markers are shown for each staining order compared to tetramer only and CCRs only (Figure 1B). Dot plots of CCR2, CCR6, CCR7, CXCR3 and CX3CR1 are shown in Figure SS2. When CCRs and tetramer were incubated together or when tetramer staining was followed by CCR staining (Figure 1B, top row), there was a clear loss of tetramer signal, compared to tetramer only staining. Staining CCRs first, followed by tetramer staining, resulted in equal detection and sensitivity compared to the optimal 'tetramer only' signal. The impact of the staining order on the performance of the anti-CCR4 antibody is shown in the lower panel of Figure 1B. Compared to CCR only staining, a shift of the total CCR4 population was observed when CCR staining was applied after tetramer staining, this was not observed when CCR staining was performed prior to tetramer staining. The same pattern was observed for the other CCRs with no loss of signal for chemokine receptors or the tetramer when chemokine receptor staining was performed prior to tetramer staining (Figure 1C, Figure S2), establishing this as the most optimal staining order.

3.3 | Intracellular staining

The next step was the addition of cytokine detection. Intracellular IFN-γ and TNF-α staining was combined with tetramer staining and performance of these markers was compared to staining with either only tetramer or only intracellular detection of cytokines (Figure 1D). The frequency of tetramer positive cells remained constant, 0.41% without vs 0.40% with intracellular cytokine staining (Figure 1D, top row). Furthermore, for both cytokines tested we did not observe loss of signal or cell frequency when tetramer staining was performed prior to the intracellular staining compared to staining without tetramer (TNF-α 6.79% vs 6.46% and IFN-γ 0.71% vs 0.71%). Thus, both abundant and less frequently produced cytokines could be detected in combination with low frequencies of tetramer positive cells and neither tetramer nor intracellular staining performance was affected by co-staining.

The optimal order for detection of chemokine receptors, tetramers and intracellular cytokines was determined based on the results described above and is depicted in Figure 2. The main staining procedure is shown in white and includes live/dead staining, blocking with human serum, the use of brilliant stain buffer and monocyte blocker, chemokine receptor and surface marker staining and finally fixation of the samples. Steps that need to be included in the workflow for tetramer staining are indicated in blue and include tetramer staining and an additional fixation step. The CD94 block is added specifically to investigate HLA-E - T cell interactions. In yellow, the standard steps for intracellular target detection are shown in the appropriate place in the staining hierarchy.

3.4 | Panel performance

In the design and application of large flow cytometry panels, such as the one described here, data analysis needs to be considered upfront. Manual gating was performed to show all main cellular subsets that could be identified on a SEB-stimulated sample (Figure 3), the unstimulated control sample is shown in Figure SS3. Irregular events, doublets and dead cells were excluded (Figure 3A-C). FCS vs SSC was used to separate monocytes and lymphocytes within the live cell population (Figure 3D). While the number of monocytes is reduced as a result of overnight stimulation, this panel could distinguish the different monocyte subsets, classical, non-classical and intermediate monocytes based on CD14 and CD16 expression (Figure 3E). Subsequent assessment of the expression of chemokine receptors CCR2 and

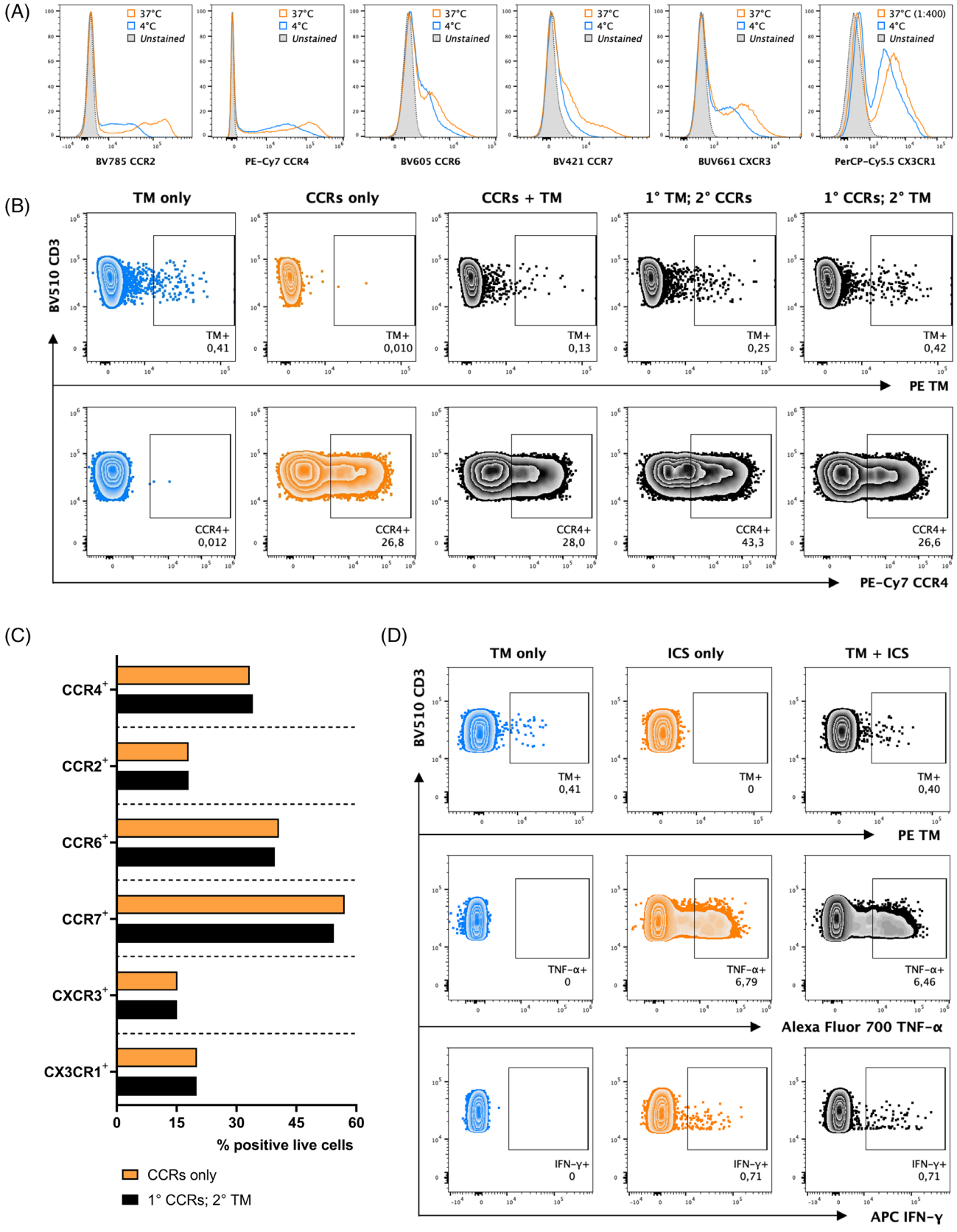

FIGURE 1 Legend on next page.

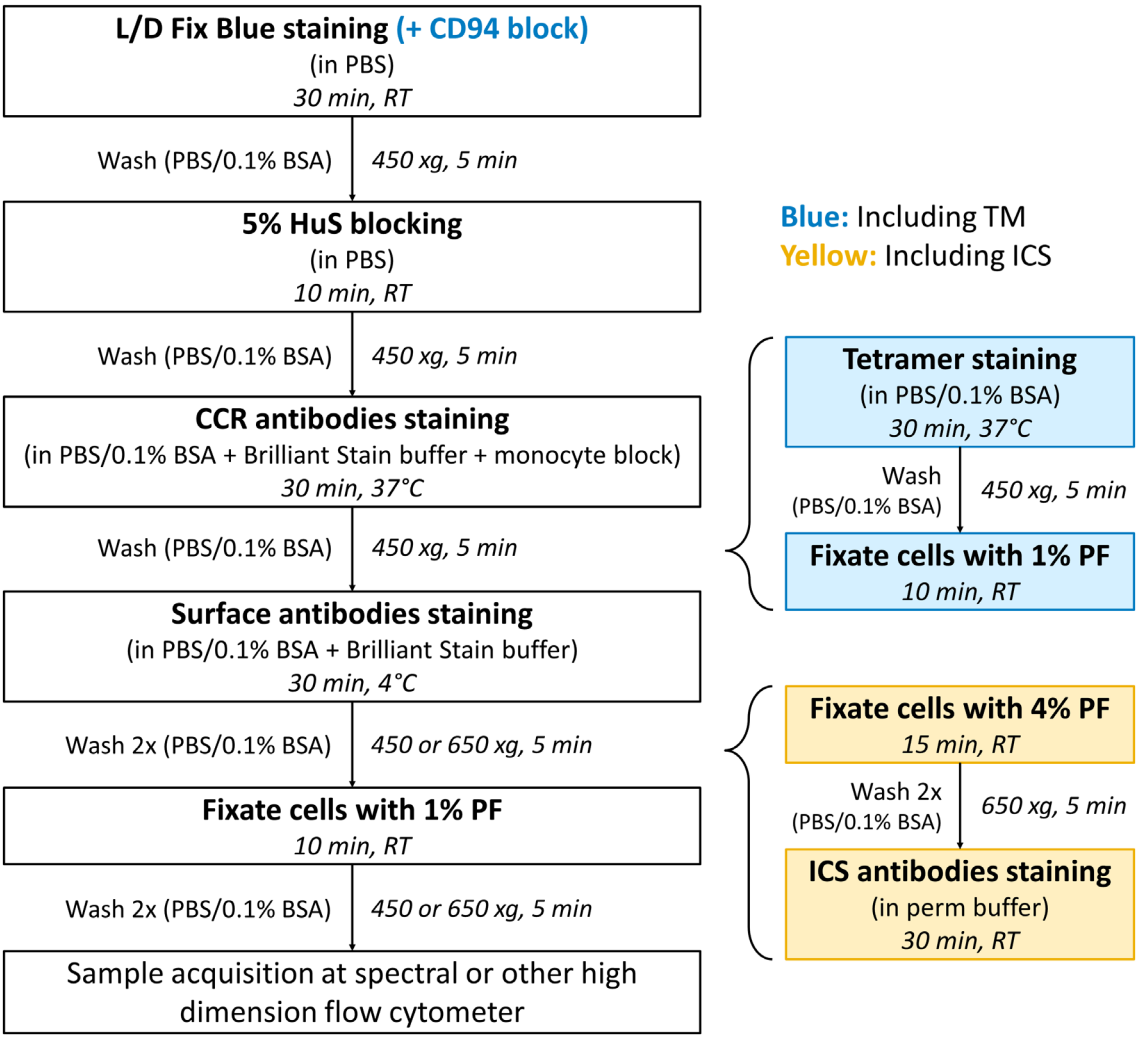

FIGURE 2 Optimal workflow for the detection of chemokine receptors, tetramers and intracellular cytokines. Based on the optimization steps performed, a workflow has been generated for the optimal staining conditions and order. In black, the primary workflow is shown. On the right, the additional steps for tetramer staining (in blue) and ICS (in yellow) are shown, which can be added to the protocol accordingly. [Color figure can be viewed at wileyonlinelibrary.com]

CX3CR1 confirmed the classification of these subsets and differential expression of LILRB receptors CD85d and CD85j could be visualized [22, 23, 29–31]. Within the lymphocyte population, B cells with CD19 and CD20 expression profiles were detected and divided into class-switched, naive or memory B cells based on CD27 and IgD (Figure 3F). Markers such as CD25, CD38 and CXCR3 could be explored in the B cell lineage to confirm or extend subset definitions. The lymphocyte subset was further explored using CD3 and CD56 to distinguish T cells, NK cells and NKT cells (Figure 3G). All major NK cell subsets were identified by assessing CD56, CD16, NKG2a and

FIGURE 1 Staining conditions and combinations tested for chemokine receptors, tetramers and cytokines. The optimal staining temperature and order was tested for chemokine receptor antibodies (CCRs), tetramers (TMs) and antibodies for intracellular cytokines, separately and combined. Data is shown for one representative donor out of three. (A) The impact of temperature on CCR staining was tested by comparing staining at 4°C (blue) and 37°C (orange). The histogram overlays represent an unstained sample (gray) and single stained samples of each antibody (1:100 dilution unless otherwise specified), gated on all live cells. (B) The effect of staining order of CCRs and TM was tested by staining PBMC samples with all surface markers including TM (blue), CCRs (orange) or CCRs and TM together in different orders (black). The top graphs represent the frequency (%) of TM^+ cells and the bottom graphs the $CCR4^+$ cells for the $CD3^+$ T-cell population. (C) The performance of all CCRs when stained prior to TM staining is plotted as a bar chart showing the frequency of positive events on all live cells for each marker (black bars), compared to staining with CCRs only (orange bars). (D) Combination of intracellular staining (ICS) and TM staining (black) was compared to ICS only (orange) and TM only (blue) with the frequency of TM^+ cells (top row), TNF-α^+ cells (middle row) and IFN-γ^+ cells (bottom row). Samples were gated on $CD3^+$ cells. [Color figure can be viewed at wileyonlinelibrary.com]

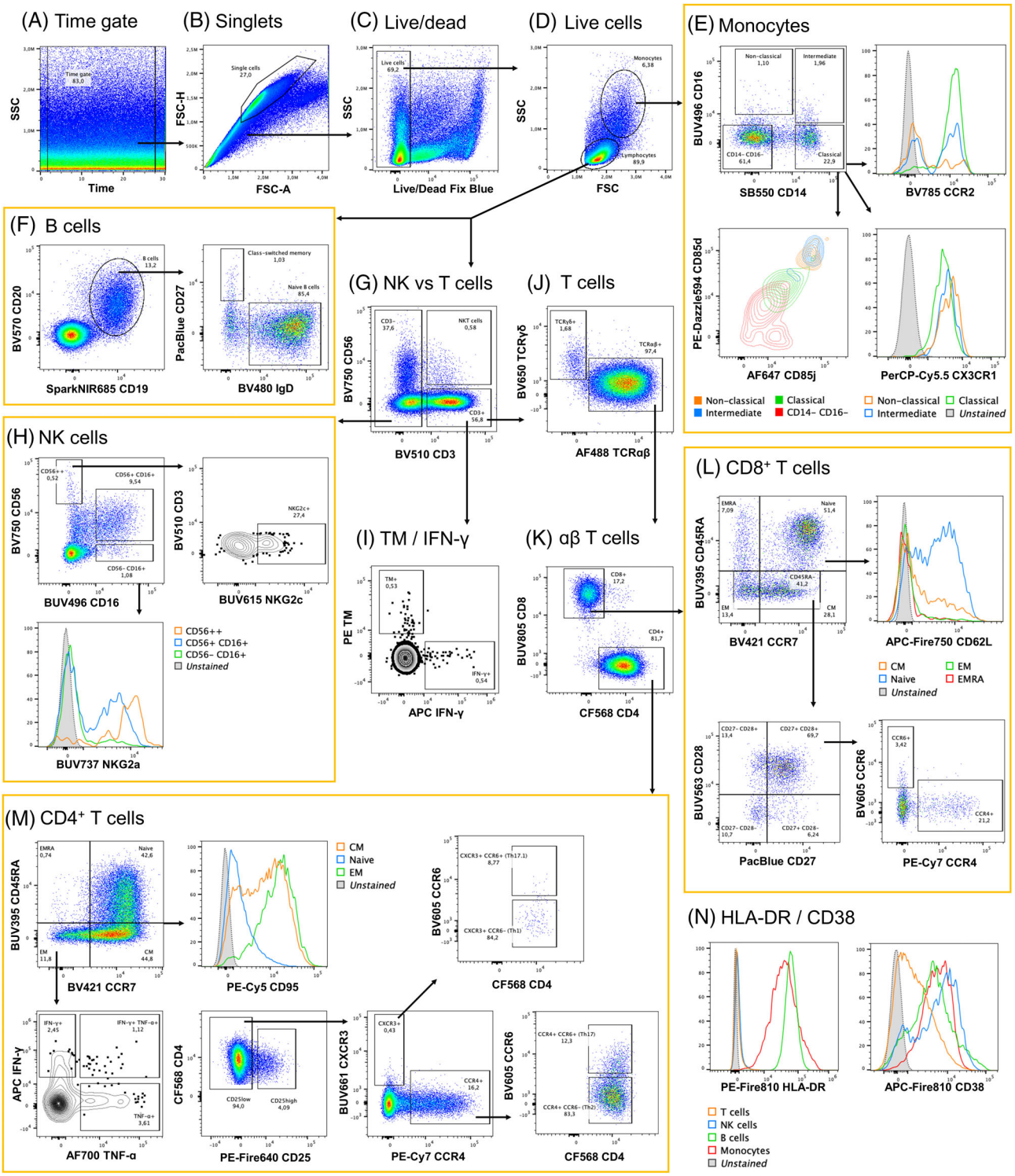

FIGURE 3 Manual gating strategy for SEB stimulated PBMC samples identifying main cell subsets. Gating for one representative donor out of 10 is shown. (A – C) Doublets, debris and dead cells exclusion based on the FSC, SSC and live dead staining. (D) Monocytes and lymphocyte separation by FSC vs SSC. (E) Monocyte subset classification and characterization based on CD14, CD16, CCR2, CX3CR1, CD85d and CD85j. (F) B cell detection by CD19 and CD20 within the lymphocyte population, including further memory subset classification by IgD and CD27. (G) CD3 and CD56 staining to separate lymphocytes into NK cells, T cells and NKT cells. (H) The different NK cell subsets based on the differential expression profiles of CD56, CD16, NKG2a and NKG2c. (I) Combination of IFN-γ detection and tetramer staining within the $CD3^+$ population. (J) $TCR\gamma\delta^+$ and $TCR\alpha\beta^+$ staining of T cells. (K) $CD4^+$ and $CD8^+$ T cells gated within the $TCR\alpha\beta^+$ population. (L – M) Classification of CD4 (L) and CD8 (M) memory subsets based on CCR7, CD45RA, CD27, CD28, CD62L and CD95, including functional differences assessed by the expression of CD25, CCR4, CCR6 and CXCR3 and cytokine detection within the effector memory subset. (N) HLA-DR and CD38 expression of all main cell subsets. [Color figure can be viewed at wileyonlinelibrary.com]

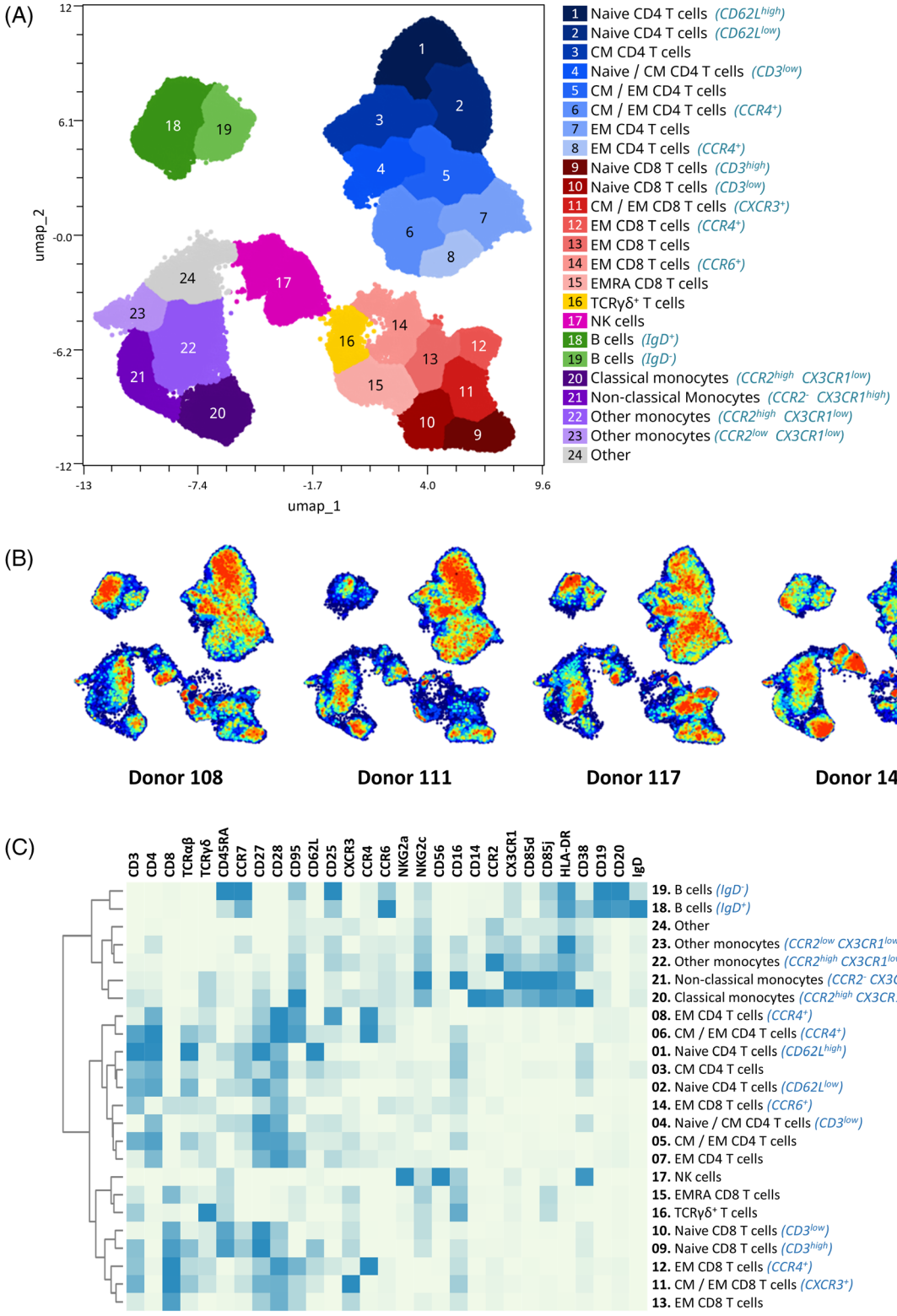

FIGURE 4 High dimensional data analysis visualizing the main subsets by UMAP and FlowSOM. Data analysis was performed on SEB stimulated PBMC samples. Only clusters with >100 cells were included for visualization. (A) All markers except for live/dead, tetramer, IFN-γ and TNF-α were included in the UMAP settings and the resulting parameters were used to cluster the data by FlowSOM. Analysis was performed on four donors. (B) Density plots of four donors representing the individual samples. (C) The 27 metaclusters generated by FlowSOM were translated into known cell populations using the clustered heatmap. [Color figure can be viewed at wileyonlinelibrary.com]

TABLE 1 Markers included in the panel. Overview of markers included per staining step and purpose of inclusion

Marker	Purpose
Live/dead staining	
Live/dead	Viability
Chemokine receptor staining	
CCR4	T cell differentiation
CCR6	T cell differentiation
CCR7	T cell differentiation
CXCR3	T cell differentiation
CCR2	Monocyte differentiation
CX3CR1	Monocyte differentiation
TM staining	
HLA-E TM	Identifying HLA-E restricted T cells
Surface staining	
CD3	T cells
CD4	T cells
CD8	T cells
TCRαβ	T cells
TCRγδ	T cells
CD45RA	T cell differentiation
CD27	T and B cell differentiation
CD28	T cell differentiation
CD95	T cell differentiation, apoptosis marker
CD62L	T cell differentiation
CD25	Activated and regulatory T and B cells
NKG2a	NK cells
NKG2c	NK cells and CD8 T cells
CD56	NK cells
CD16	Monocyte and NK cell differentiation
CD14	Monocytes
CD85d	Monocytes and B cells
CD85j	Monocytes and B cells
HLA-DR	T cell and monocyte activation
CD38	T cell, B cell and monocyte activation
CD19	B cells
CD20	B cells
IgD	B cell differentiation
Intracellular staining	
IFN-γ	Cytokine
TNF-α	Cytokine

NKG2c receptor expression (Figure 3H) [18]. Within the $CD3^+$ population, detection of IFN-γ and tetramer staining is compatible (Figure 3I). Within the T cell subset, TCRαβ T cells (97.4% of $CD3^+$ cells) and TCRγδ T cells (1,68% of $CD3^+$ cells) were identified (Figure 3J). TCRαβ positive cells were then classified as $CD8^+$ T cells (Figure 3K,L) and $CD4^+$ T cells (Figure 3K,M). Each of these subsets could be divided into naive, central memory, effector memory and effector cells by studying the expression of CD45RA, CCR7 and/or CD27; addition of CD28 and CD62L was used to dissect further subsets within the central memory and effector memory populations (Figure 3L,M). Within the $CD4^+$ effector memory subset, presence of IFN-γ (2,45%), TNF-α (3,61%) or both (1.12%) are shown (Figure 3M). Regulatory T cells were identified by $CD25^{high}$ expression (Figure 3M) and characterization of more T cell subsets with functional differences included CD95, CCR4, CCR6 and CXCR3 (Figure 3L,M). Expression of HLA-DR and CD38 on the main lineages is shown in Figure 3N. PMA and ionomycin are often used as strong T cell stimulus, therefore panel performance following this stimulus was also assessed (Figure S4). All populations could still be identified, but CD3, CD4 and CD62L on T cells, NKG2c on NK cells, and CD16 on both monocytes and NK cells were downregulated substantially in line with reports in the literature [35, 36]. As expected, PMA and ionomycin stimulation resulted in a large cytokine producing T cell population.

While it is possible to manually gate the data produced by high-dimensional panels, as demonstrated in Figure 3, analysis algorithms can be used to achieve more comprehensive data. Here OMIQ software was used to visualize all main subsets, that were also characterized by manual analysis in Figure 3, through UMAP for dimensionality reduction and FlowSOM as unsupervised clustering method (Figure 4A). These data are based on the combination of four different donors (density plots shown in Figure 4B). The following clusters were identified: $CD4^+$ (metacluster 1 to 8) and $CD8^+$ (metacluster 9 to 15), $TCR\gamma\delta^+$ T cells (metacluster 16), NK cells (metacluster 17), B cells (metacluster 18 and 19) and monocytes (metacluster 20 to 23). The unique (memory) subsets of the main cellular lineages were captured in a clustered heatmap (Figure 4C).

4 | DISCUSSION

Multi parameter (spectral) flow cytometry is needed to study and understand the diversity of the immune response in relation to health, disease, treatment or responses to vaccination. Recently, the access to tools and technology has increased and multiple 30+ parameter flow cytometry panels for human PBMC samples have been published. However, so far, panels combining broad immunophenotyping with readouts of cellular function in response to stimulation are scarce. When designing flow cytometry panels, selection of the optimal combination of markers and fluorophores yielding high quality data is one of the main concerns (this has been described extensively elsewhere [3, 4, 37]). However, optimizing staining conditions during implementation of the panel is equally important. Many markers have specific staining requirements that need to be performed in a certain order to retrieve data of high quality. This paper describes an optimized workflow to stain human PBMC samples with a 32-color panel consisting of surface markers, chemokine receptors, MHC–peptide tetramers and intracellular cytokines.

It is well established that staining certain chemokine receptors at 37°C improves signal [38–40], which we have confirmed for CCR2, CCR4, CCR6, CCR7 and CXCR3 in our panel, while the CX3CR1 expression level was unaffected by temperature. HLA-E-peptide complexes also require staining at 37°C and fixation immediately thereafter to retain signal [12, 34]. Fixation may introduce possible loss of detection of surface markers but after HLA-E peptide tetramer staining we did not experience noteworthy loss of surface markers or intensity based on the fixation. Staining order significantly impacted detection of TM+ events; staining of CCRs simultaneously with tetramer or following tetramer negatively impacted detection of tetramer specific T cell receptors. Our data has shown that if tetramer staining was performed after CCR staining, even low frequency peptide specific HLA-E restricted T cells could be detected. Intracellular cytokine staining after tetramer staining did not impact the quality of either tetramer or cytokine detection compared to staining for these markers separately. Cytokine and tetramer double positive events are minimal here as stimulation was performed with SEB to boost overall cytokine production rather than activating *Mtb*-specific cells detected by the tetramer, which are rare in healthy donors in a low TB endemic country like the Netherlands. After stimulation, we did observe reduced quality of CXCR3 and CCR6 staining compared to the unstimulated sample, but this is likely due to the lack of receptor recycling specifically for these chemokine receptors [41, 42].

When working with large panels it is crucial to understand the dynamics of marker interactions within the panel and control for assay variations in order to obtain robust results. This requires establishment of proper controls for the flowcytometric analyzer used and acquisition of the cells, e.g. fluorescence minus one controls (FMO), reference controls and, if possible, to consider including an autofluorescence control for monocytes. With regards to these controls, we found that acquiring a sufficient number of cells to ensure proper identification of the positive population, particularly for markers with small positive percentages, was essential for accurate unmixing. In addition, in our hands, using cells as staining controls gave superior unmixing results for all markers compared to beads, although others have reported success with bead controls for certain markers [5]. Addition of the brilliant stain buffer and a monocyte blocker improved the quality of the data by overcoming issues with the chemical properties of the antibodies. The brilliant stain buffer prevents interactions between different brilliant violet and brilliant UV dyes whereas the monocyte blocker particularly prevents non-specific binding of cyanine-based tandem dyes to monocytes. Furthermore, for tetramer staining and cytokine detection, it is important to evaluate the responses within a consistent timeframe after staining. As demonstrated, the aforementioned optimization steps for this panel resulted in high-quality data with separation of cell phenotypes both by manual gating and unsupervised clustering analysis.

Our 32-color panel includes chemokine receptors and surface markers as well as more functional tetramer and cytokine detection, allowing identification of all main cellular lineages within one sample with simultaneous antigen specific and cytokine readout. We believe such panels are required to study the repertoire of immune cells and will contribute to expanding our understanding of disease states, treatment effects or vaccine induced responses.

ACKNOWLEDGMENTS

The authors thank Kees LMC Franken (Dept Infectious Diseases and Immunology, Leiden University Medical Center) for preparation of HLA-E tetramers and the operators of the Flow cytometry Core Facility from Leiden University Medical Center for their assistance with the flow cytometry analysers and technical support. Research reported in this publication was supported by the National Institute of Allergy and Infectious Diseases of the National Institutes of Health under award number R01AI141315 (to Tom H.M. Ottenhoff and Simone A. Joosten). Paula Niewold is supported by the International Society for the Advancement of Cytometry (ISAC) Marylou Ingram Scholars Program.

PEER REVIEW

The peer review history for this article is available at https://publons.com/publon/10.1002/cyto.a.24727.

DATA AVAILABILITY STATEMENT

FCS files for the data presented in this manuscript are available on Flow Repository: FR-FCM-Z6YH.

CONFLICT OF INTEREST STATEMENT

The authors declare no conflict of interest.

ORCID

Paula Niewold https://orcid.org/0000-0002-9614-4601

REFERENCES

1. Picot J, Guerin CL, Le Van KC, Boulanger CM. Flow cytometry: retrospective, fundamentals and recent instrumentation. Cytotechnology. 2012;64(2):109–30.
2. Nolan JP. The evolution of spectral flow cytometry. Cytometry A. 2022;101:812–7.
3. Ashhurst TM, Smith AL, King NJC. High-dimensional fluorescence cytometry. Curr Protoc Immunol. 2017;119:5 8 1-5 8 38.
4. Ferrer-Font L, Pellefigues C, Mayer JU, Small SJ, Jaimes MC, Price KM. Panel design and optimization for high-dimensional immunophenotyping assays using spectral flow cytometry. Curr Protoc Cytom. 2020;92(1):e70.
5. Park LM, Lannigan J, Jaimes MC. OMIP-069: forty-color full Spectrum flow cytometry panel for deep immunophenotyping of major cell subsets in human peripheral blood. Cytometry A. 2020;97(10):1044–51.
6. Staser KW, Eades W, Choi J, Karpova D, DiPersio JF. OMIP-042: 21-color flow cytometry to comprehensively immunophenotype major lymphocyte and myeloid subsets in human peripheral blood. Cytometry A. 2018;93(2):186–9.
7. Payne K, Li W, Salomon R, Ma CS. OMIP-063: 28-color flow cytometry panel for broad human immunophenotyping. Cytometry A. 2020;97(8):777–81.
8. Nogimori T, Sugawara Y, Higashiguchi M, Murakami H, Akita H, Takahama S, et al. OMIP 078: a 31-parameter panel for comprehensive immunophenotyping of multiple immune cells in human peripheral blood mononuclear cells. Cytometry A. 2021;99(9):893–8.

9. Maecker HT. Cytokine measurement by flow cytometry. In: Detrick B, Schmitz JL, Hamilton RG, editors. Manual of molecular and clinical laboratory immunology. 8th ed. Washinton, DC: ASM Press; 2016. p. 338–42.
10. Roederer M, Brenchley JM, Betts MR, De Rosa SC. Flow cytometric analysis of vaccine responses: how many colors are enough? Clin Immunol. 2004;110(3):199–205.
11. Chattopadhyay PK, Melenhorst JJ, Ladell K, Gostick E, Scheinberg P, Barrett AJ, et al. Techniques to improve the direct ex vivo detection of low frequency antigen-specific CD8+ T cells with peptide-major histocompatibility complex class I tetramers. Cytometry A. 2008; 73(11):1001–9.
12. Prezzemolo T, van Meijgaarden KE, Franken K, Caccamo N, Dieli F, Ottenhoff THM, et al. Detailed characterization of human mycobacterium tuberculosis specific HLA-E restricted CD8(+) T cells. Eur J Immunol. 2018;48(2):293–305.
13. Voogd L, Ruibal P, Ottenhoff THM, Joosten SA. Antigen presentation by MHC-E: a putative target for vaccination? Trends Immunol. 2022; 43(5):355–65.
14. Ottenhoff THM, Joosten SA. Mobilizing unconventional T cells. Science. 2019;366(6463):302–3.
15. Joosten SA, Sullivan LC, Ottenhoff TH. Characteristics of HLA-E restricted T-cell responses and their role in infectious diseases. J Immunol Res. 2016;2016:2695396–11.
16. Maecker HT, McCoy JP, Nussenblatt R. Standardizing immunophenotyping for the human immunology project. Nat Rev Immunol. 2012; 12(3):191–200.
17. Jiang Y, Cui X, Cui C, Zhang J, Zhou F, Zhang Z, et al. The function of CD3+CD56+ NKT-like cells in HIV-infected individuals. Biomed Res Int. 2014;2014:863625.
18. Montaldo E, Del Zotto G, Della Chiesa M, Mingari MC, Moretta A, De Maria A, et al. Human NK cell receptors/markers: a tool to analyze NK cell development, subsets and function. Cytometry A. 2013;83(8): 702–13.
19. Liechti T, Roederer M. OMIP-051 - 28-color flow cytometry panel to characterize B cells and myeloid cells. Cytometry A. 2019;95(2):150–5.
20. Klein U, Rajewsky K, Kuppers R. Human immunoglobulin (Ig)M+IgD+ peripheral blood B cells expressing the CD27 cell surface antigen carry somatically mutated variable region genes: CD27 as a general marker for somatically mutated (memory) B cells. J Exp Med. 1998; 188(9):1679–89.
21. Ziegler-Heitbrock L, Ancuta P, Crowe S, Dalod M, Grau V, Hart DN, et al. Nomenclature of monocytes and dendritic cells in blood. Blood. 2010;116(16):e74–80.
22. Sampath P, Moideen K, Ranganathan UD, Bethunaickan R. Monocyte subsets: phenotypes and function in tuberculosis infection. Front Immunol. 2018;9:1726.
23. Kapellos TS, Bonaguro L, Gemund I, Reusch N, Saglam A, Hinkley ER, et al. Human monocyte subsets and phenotypes in major chronic inflammatory diseases. Front Immunol. 2019;10:2035.
24. Mahnke YD, Brodie TM, Sallusto F, Roederer M, Lugli E. The who's who of T-cell differentiation: human memory T-cell subsets. Eur J Immunol. 2013;43(11):2797–809.
25. Appay V, van Lier RA, Sallusto F, Roederer M. Phenotype and function of human T lymphocyte subsets: consensus and issues. Cytometry A. 2008;73(11):975–83.
26. Geginat J, Paroni M, Facciotti F, Gruarin P, Kastirr I, Caprioli F, et al. The CD4-centered universe of human T cell subsets. Semin Immunol. 2013;25(4):252–62.
27. Ahmed R, Roger L, Costa Del Amo P, Miners KL, Jones RE, Boelen L, et al. Human stem cell-like memory T cells are maintained in a state of dynamic flux. Cell Rep. 2016;17(11):2811–8.
28. Shiroishi M, Tsumoto K, Amano K, Shirakihara Y, Colonna M, Braud VM, et al. Human inhibitory receptors Ig-like transcript 2 (ILT2) and ILT4 compete with CD8 for MHC class I binding and bind preferentially to HLA-G. Proc Natl Acad Sci U S A. 2003;100(15):8856–61.
29. Cosman D, Fanger N, Borges L, Kubin M, Chin W, Peterson L, et al. A novel immunoglobulin superfamily receptor for cellular and viral MHC class I molecules. Immunity. 1997;7(2):273–82.
30. Fanger NA, Cosman D, Peterson L, Braddy SC, Maliszewski CR, Borges L. The MHC class I binding proteins LIR-1 and LIR-2 inhibit fc receptor-mediated signaling in monocytes. Eur J Immunol. 1998;28(11):3423–34.
31. Dechavanne C, Nouatin O, Adamou R, Edslev S, Hansen A, Meurisse F, et al. Placental malaria is associated with higher LILRB2 expression in monocyte subsets and lower anti-malarial IgG antibodies during infancy. Front Immunol. 2022;13:909831.
32. Ruibal P, Franken KLMC, van Meijgaarden KE, van Wolfswinkel M, Derksen I, Scheeren FA, et al. Identification of novel HLA-E-binding Mtb-derived epitopes through improved prediction models. J Immunol. 2022;209(8):1555–65.
33. Joosten SA, van Meijgaarden KE, van Weeren PC, Kazi F, Geluk A, Savage ND, et al. Mycobacterium tuberculosis peptides presented by HLA-E molecules are targets for human CD8 T-cells with cytotoxic as well as regulatory activity. PLoS Pathog. 2010;6(2):e1000782.
34. Yang H, Rei M, Brackenridge S, Brenna E, Sun H, Abdulhaqq S, et al. HLA-E-restricted, gag-specific CD8(+) T cells can suppress HIV-1 infection, offering vaccine opportunities. Sci Immunol. 2021;6(57):eabg1703.
35. Romee R, Foley B, Lenvik T, Wang Y, Zhang B, Ankarlo D, et al. NK cell CD16 surface expression and function is regulated by a disintegrin and metalloprotease-17 (ADAM17). Blood. 2013;121(18):3599–608.
36. Baran J, Kowalczyk D, Ozog M, Zembala M. Three-color flow cytometry detection of intracellular cytokines in peripheral blood mononuclear cells: comparative analysis of phorbol myristate acetate-ionomycin and phytohemagglutinin stimulation. Clin Diagn Lab Immunol. 2001;8(2):303–13.
37. Holmberg-Thyden S, Gronbaek K, Gang AO, El Fassi D, Hadrup SR. A user's guide to multicolor flow cytometry panels for comprehensive immune profiling. Anal Biochem. 2021;627:114210.
38. Berhanu D, Mortari F, De Rosa SC, Roederer M. Optimized lymphocyte isolation methods for analysis of chemokine receptor expression. J Immunol Methods. 2003;279(1–2):199–207.
39. Anselmo A, Mazzon C, Borroni EM, Bonecchi R, Graham GJ, Locati M. Flow cytometry applications for the analysis of chemokine receptor expression and function. Cytometry A. 2014;85(4):292–301.
40. Le Brocq ML, Fraser AR, Cotton G, Woznica K, McCulloch CV, Hewitt KD, et al. Chemokines as novel and versatile reagents for flow cytometry and cell sorting. J Immunol. 2014;192(12):6120–30.
41. Meiser A, Mueller A, Wise EL, McDonagh EM, Petit SJ, Saran N, et al. The chemokine receptor CXCR3 is degraded following internalization and is replenished at the cell surface by de novo synthesis of receptor. J Immunol. 2008;180(10):6713–24.
42. Lu MY, Lu SS, Chang SL, Liao F. The phosphorylation of CCR6 on distinct ser/Thr residues in the carboxyl terminus differentially regulates biological function. Front Immunol. 2018;9:415.

SUPPORTING INFORMATION

Additional supporting information can be found online in the Supporting Information section at the end of this article.

How to cite this article: van Wolfswinkel M, van Meijgaarden KE, Ottenhoff THM, Niewold P, Joosten SA. Extensive flow cytometric immunophenotyping of human PBMC incorporating detection of chemokine receptors, cytokines and tetramers. Cytometry. 2023;103(7):600–10. https://doi.org/10.1002/cyto.a.24727